(Received 25 February 2026, Accepted 2 April 2026, Scheduled 17 April 2026)

Conception and Fabrication of a Metamaterials Based Patch Antenna for Biomedical Applications

Younes Siraj[1,*], Jaouad Foshi[1], Youssef Khardioui[1], Souad Akkader[2], Youssef Mejdoub[3], Kaoutar Saidi Alaoui[4], and Abdennaceur Baghdad[2]

[1] *ISMSE Laboratory, Faculty of Sciences and Technology, Errachidia, Moulay Ismail University of Meknes, Morocco*
[2] *Laboratory of Engineering Sciences and Biosciences, Faculty of Science and Techniques Hassan II University Mohammedia, Morocco*
[3] *Laboratory of Networks, Computer Science, Telecommunication & Multimedia (RITM) Higher School of Technology, Hassan II University, Casablanca, Morocco*
[4] *Higher School of Technology, Ibn Zohr University, Morocco*

ABSTRACT: This study presents the design, simulation, and fabrication of a compact patch antenna with metamaterials, dedicated to biomedical applications. The proposed antenna was implemented on an FR4 substrate and resonated at a center frequency of 2.48 GHz. By the integration of metamaterial (MTM) unit cells as the primary radiating element, the design achieves performance improvements compared with traditional patch antennas. The return loss was reduced from -13.45 to -67.20 dB, which indicates improved impedance matching. In addition, the antenna showed enhanced radiation characteristics, with a gain of 1.96 dB and a directivity of 3.10 dB. As the antenna was designed for biomedical use, specific absorption rate (SAR) analysis was conducted to ensure compliance with safety standards. A prototype of the antenna was fabricated to validate the simulation results, and the measured results matched the simulations, which confirms the reliability of the suggested design. The simulation results were obtained using HFSS and CST. Overall, the results demonstrate that the proposed metamaterials-based antenna is a strong candidate for integration into biomedical devices.

1. INTRODUCTION

The continuous development of antennas has attracted attention in many fields, including medicine. In our current era, wearable antennas have become essential for ensuring the continuous monitoring of patient health [1], medical telemetry systems [2], facilitating easier and safer surveillance of patient health [3]. Designing antennas for the medical field remains a difficult and complex matter due to the sensitivity of the field and its requirements, such as small size and flexibility, in addition to ensuring the safe use of these antennas to avoid any side effects that could negatively affect the user's health.

Over time, patch antennas have gained significant attention in biomedical applications due to their small size, low cost, and ease of integration with flexible and biocompatible substrates [4–6]. With all these advantages, traditional patch antennas face several challenges, such as limited bandwidth, low gain, and reduced efficiency, which limit their performance in biomedical environments that demand high characteristics. In order to solve these problems, various strategies have been proposed, including substrate modification [7], defected ground structures (DGSs) [8, 9], and integration of metamaterial (MTM) [10–12]. Among the suggested solutions, MTMs have shown great potential for improving the performance of conventional antennas. Owing to their unique electromagnetic properties, such as negative permittivity and/or permeability [13], MTM can improve the impedance matching, reduce antenna size, and enhance radiation characteristics. These capabilities make MTMs a suitable solution for the enhancement of antennas designed for biomedical applications.

In [14], the gain enhancement of a patch antenna using a grounded MTM is reported, where the integration of MTM results in an increase in the gain of approximately 3 dB. Another study for the gain enhancement using an I-shaped MTM superstrate was proposed in [15], in which an improvement in the gain of the antenna by 74.28% was achieved. In [16], an MTM-based patch antenna is introduced, and the proposed configuration resonates at 3.5 GHz with a reflection coefficient of -40 dB and a bandwidth of 210.2 MHz. The MTM integration results in a bandwidth enhancement of 151.3 MHz. Furthermore, the gain was increased by 2.23 dBi. In [17], a high magnetic permeability MTM superstrate for a patch antenna is presented, and the antenna operates at 2.4 GHz with a gain enhancement from 2.8 to 7.8 dB by integrating an single-ring split-ring resonator (SRSRR) superstrate.

In contrast to earlier methods, our study introduces a fresh approach by using MTM itself as the radiating element of the antenna, instead of placing it underneath the patch or in the ground plane. The proposed strategy helps to maintain a compact size and also preserves strong electromagnetic performance. By the integration of the MTM in this way, we were able to enhance impedance matching, enhance radiation efficiency, and reduce the overall size of the antenna, all while maintaining flexibility. Compared to traditional patch antenna

* Corresponding author: Younes Siraj (sirajyounes95@gmail.com).

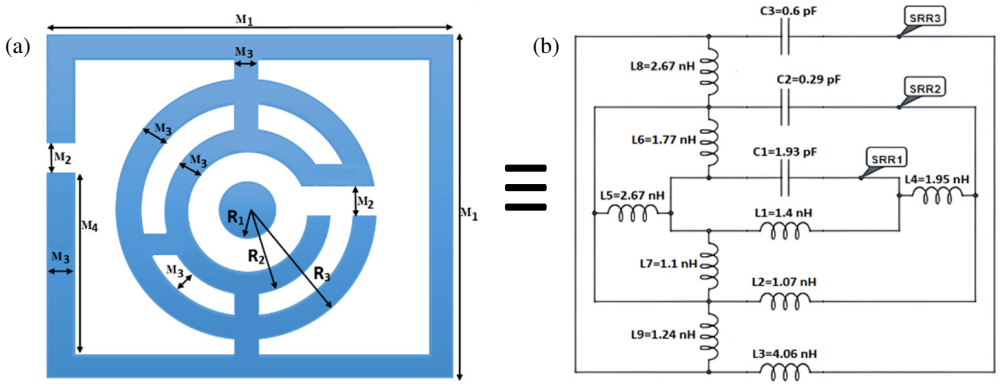

FIGURE 1. Unit cell (a) design, (b) equivalent circuit.

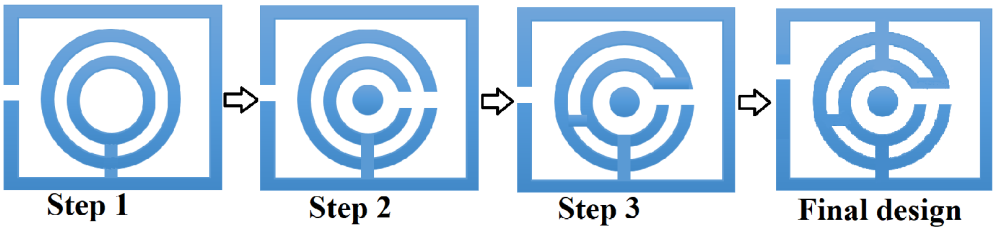

FIGURE 2. Unit cell design development.

designs, our results show clear improvements in the return loss, gain, and directivity. In order to validate the simulation results, we also fabricated the antenna prototype and measured its performance, which confirmed the effectiveness of our design.

The rest of this work is organized as follows. Section 2 provides a detailed discussion of the use of patch antennas in biomedical applications. Section 3 describes the simulation setup and an MTM-based antenna configuration. Section 4 presents a parametric study. Section 5 discusses and compares the simulated and experimental results, validating the proposed design. Finally, Section 6 presents a conclusion and future research directions.

2. MTM AND PATCH ANTENNA STRUCTURES

2.1. MTM Unit Cell

This section presents the structure of our proposed MTM unit cell. The design comprised a square resonator with a total size of $28 \times 28\,\text{mm}^2$, which acts as the antenna radiating element. In complement, two circular split-ring resonators with outer and inner radii of 10 mm and 6 mm, respectively, were integrated. These resonators were placed in a way that minimizes the electromagnetic interference and unwanted coupling. To reduce mutual interactions, a 2 mm spacing is maintained among all three resonators. Additionally, as illustrated in Fig. 1(a), each resonator included a 2 mm slit, which helped to fine-tune the resonance behavior and enhance the characteristics of the unit cell. The equivalent circuit of the suggested unit cell is presented in Fig. 1(b). The outer, middle, and inner rings of the complementary aplit-eing resonator (CSRR) are represented by three inductances ($L1$–$L3$) in combination with capacitors ($C1$–$C3$), while the connections between the rings are modeled by additional inductances ($L5$–$L9$). Specifically, the ring radii and widths determine the values of the inductances and coupling capacitances, while the gap spacing between the rings defines the capacitances. This configuration is specially designed to enhance the patch antenna performances while keeping a compact size and minimized losses. The unit cell dimensions are listed in Table 1.

TABLE 1. Suggested MTM unit cell dimensions.

Parameters	Values (mm)	Parameters	Values (mm)
$M1$	28	$R1$	2
$M2$	2	$R2$	6
$M3$	2	$R3$	10
$M4$	12		

In order to obtain the final unit cell design, we went through four steps, as illustrated in Fig. 2. Each stage presents some adjustments and modifications to the dimensions, resonator placements, and structural features, which optimize the unit cell characteristics in terms of the resonance frequency and the coupling among the three rings. Step 1 represents the initial square patch resonator with two circular rings, where the dimensions are calculated using classical patch antenna equations to achieve the desired resonant frequency. Step 2 introduces an opening in the two circular split-ring resonators, providing additional inductive and capacitive loading to enhance bandwidth and miniaturize the structure. Step 3 incorporates some connecting strips among the rings, which fine-tunes the resonance, improves current distribution, and optimizes impedance matching. The final design integrates all these modifications and introduces an ad-

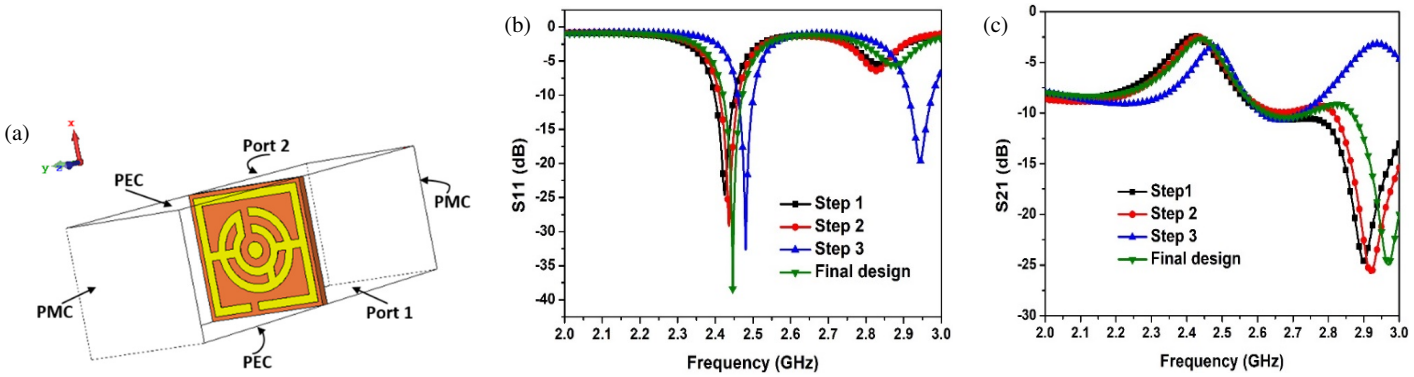

FIGURE 3. (a) Unit cell simulation setup, (b) unit cell S_{11} and (c) unit cell S_{21}.

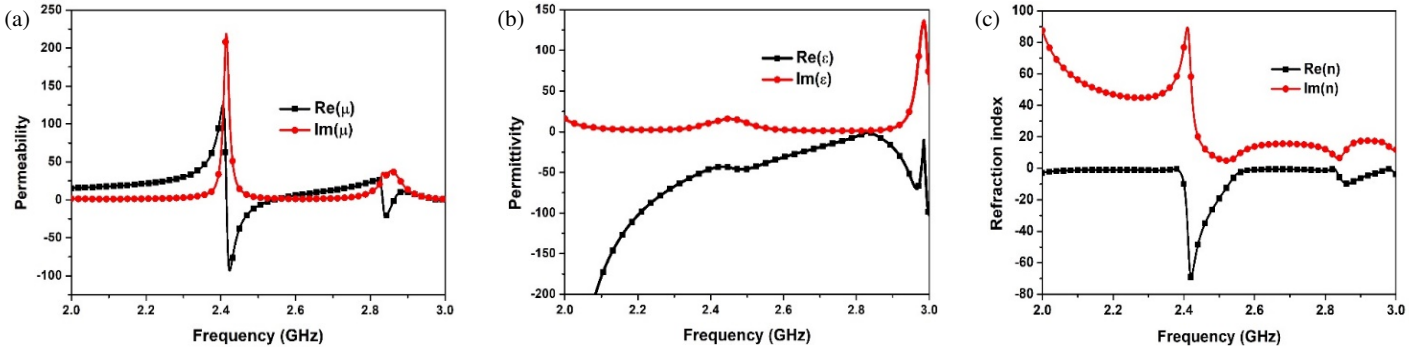

FIGURE 4. Unit cell; (a) mu, (b) epsilon, and (c) refraction index.

ditional strip connecting the square ring to the circular rings from the upper side, resulting in a compact unit cell with enhanced electromagnetic performance suitable for integration as the radiating element in the proposed antenna.

Figure 3 illustrates the simulation setup used to extract the characteristics of our proposed unit cell. Along the Y-axis, two ports are placed to deliver the input signal and perform the necessary excitation for the unit cell. To ensure accurate electromagnetic field distribution and boundary conditions, perfect electric and perfect magnetic boundaries are placed along the X- and Z-axes, respectively. This setup allows for the determination of the unit cell's resonance behavior, impedance characteristics, and overall performance of the unit cell in the designed configuration. The obtained S_{11} and S_{21} results obtained for each stage of the design process are presented in Fig. 3(a) and Fig. 3(b), respectively. These results provide insights into the performance improvements made throughout the optimization process.

After getting S_{11} and S_{21} using the High Frequency Structure Simulator (HFSS) software, we used MATLAB to extract the unit cell parameters including mu(1), epsilon(2), and refraction index(3), using the Nicolson-Ross-Weir (NRW) method which is a standard technique that calculates the effective electromagnetic properties of a material from its reflection and transmission coefficients. By relating S_{11} and S_{21} to the material's impedance and refractive index, the method allows the accurate determination of frequency-dependent permittivity, permeability, and refractive index of the unit cell. The extraction was performed using the following equations [18]:

$$\mu = \frac{2}{jkh} \cdot \frac{1 - S_{21} + S_{11}}{1 + S_{21} - S_{11}} \tag{1}$$

$$\varepsilon = \frac{2}{jkh} \cdot \frac{1 - S_{21} - S_{11}}{1 + S_{21} + S_{11}} \tag{2}$$

$$n = \sqrt{\varepsilon\mu} \tag{3}$$

The obtained results are presented in Fig. 4. In Fig. 4(a), the real and imaginary parts of the permeability are shown. The real part indicates a negative value around 2.4 GHz, accompanied by a peak in the imaginary part, which indicates a magnetic resonance behavior. Fig. 4(b) illustrates the real and imaginary parts of the permittivity, which achieved negative values in the entire studied frequency range from 2 to 3 GHz, confirming the presence of an electric resonance. Additionally, Fig. 4(c) presents the real and imaginary components of the refractive index, in which the real part presents a negative value near 2.4 GHz, demonstrating the negative index characteristic of the unit cell.

2.2. Suggested Antenna Configuration

The proposed MTM-based patch antenna has compact dimensions of $66 \times 60\,\text{mm}^2$ designed for biomedical applications. As shown in Fig. 5(b), the antenna contained two identical MTM units as the radiating elements, implemented horizontally on an FR4 material substrate with a dielectric constant of 4.4, loss

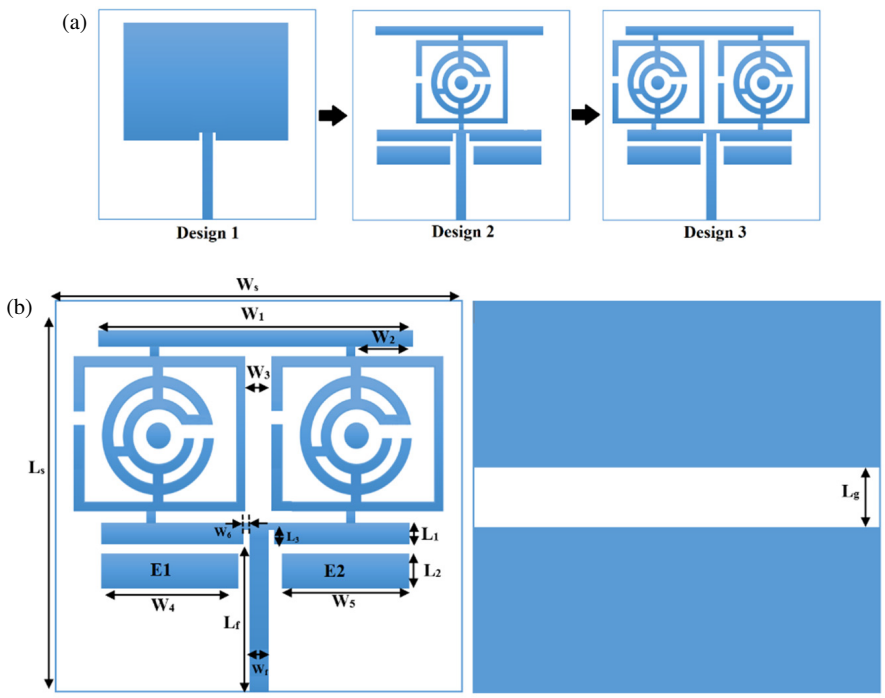

FIGURE 5. Patch antenna. (a) Design process. (b) Final structure design.

TABLE 2. Suggested antenna dimensions.

Parameters	Values (mm)	Parameters	Values (mm)	Parameters	Values (mm)
W_S	66	W_3	2	L_1	4
L_S	60	W_4	23	L_2	8
W_1	52	W_5	22	L_3	3
W_2	15.5	W_6	1	L_g	10
W_f	14	L_f	2		

tangent of 0.022, and thickness of 1.6 mm. A microstrip feed line of $14 \times 2\,\text{mm}^2$ is used to excite the antenna, while two small slots are inserted between the feed line and the patch in order to enhance the impedance matching and minimize reflection losses. In addition, a rectangular slot of $66 \times 10\,\text{mm}^2$ is incorporated into the ground plane, which improved the current distribution and impedance characteristics. Moreover, two parasitic rectangular elements, E1 and E2, with dimensions of $23 \times 8\,\text{mm}^2$ and $22 \times 8\,\text{mm}^2$, respectively, were placed beneath the unit cells to enhance the gain and radiation efficiency. The dimensions of E1 and E2 were initially selected and subsequently refined through parametric analysis in HFSS, evaluating their impact on gain, radiation efficiency, and impedance matching, until the final dimensions achieving the best overall antenna performance were determined. All design modifications led to a compact, high-performance antenna designed for biomedical applications. The initial design dimensions were obtained using a standard patch antenna in Equations (4), (5), (6), and (7), where C is the speed of light, and h is the substrate thickness, followed by iterative simulations in HFSS to adjust the resonant frequency and optimize overall performance. The design evolution process is illustrated in Fig. 5(a), and the complete dimensions are summarized in Table 2.

$$W_p = \frac{c}{2f_r}\sqrt{\frac{2}{\varepsilon_r + 1}} \tag{4}$$

$$L_{reff} = \frac{c}{2f_r\sqrt{\varepsilon_{reff}}} \tag{5}$$

$$L_p = L_{eff} - 2\Delta L \tag{6}$$

$$\Delta L = 0.412h\,\frac{(\gamma_{reff} + 0.3)\left(\frac{w}{h} + 0.264\right)}{(\gamma_{reff} - 0.258)\left(\frac{w}{h} + 0.8\right)} \tag{7}$$

3. PARAMETRIC STUDY

3.1. Effect of Distance between the Two Cells

A parametric study was performed by varying the distance between the two unit cells (W_3) from 1 to 4 mm in 1 mm increments. The objective was to investigate the effect of inter-element spacing on the antenna's reflection characteristics. As

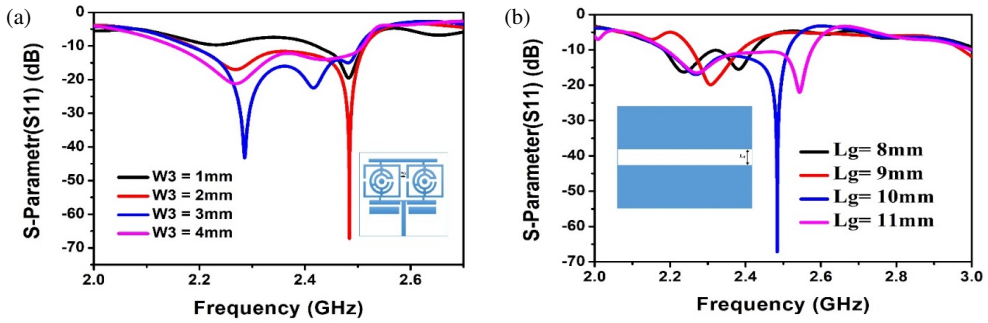

FIGURE 6. S_{11} for different (a) values of W_3, (b) values of L_g.

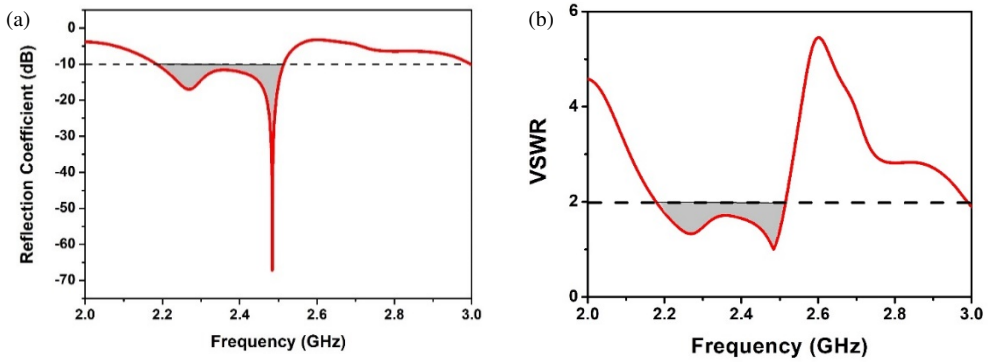

FIGURE 7. Suggested antenna; (a) S_{11} and (b) VSWR.

illustrated in Fig. 6(a), the variation in W_3 influenced the reflection coefficient. Of the tested values, a 2 mm spacing resulted in optimal performance, achieving a minimum S_{11} of -67.20 dB at 2.48 GHz.

3.2. Effect of Distance L_g

To evaluate the impact of the inserted slot length in the ground plane on the antenna characteristics, an analysis study was performed by changing the parameter L_g from 8 to 11 mm in 1 mm increments. The results, presented in Fig. 6(b), demonstrate a big impact of L_g on the impedance matching of the antenna. As L_g increases, a remarkable improvement in S_{11} was observed, which indicates enhanced antenna performance. The optimal configuration is obtained with $L_g = 10$ mm, which provided the best impedance matching and overall reflection performance.

4. RESULTS AND DISCUSSION

4.1. Return Loss and VSWR

The simulated reflection coefficient and voltage standing wave ratio are illustrated in Fig. 7(a) and Fig. 7(b), respectively. The antenna showed an enhanced reflection coefficient of -67.20 dB, accompanied by a voltage standing wave ratio (VSWR) of 1.01, which indicates a very good level of impedance matching between the antenna and the feed line. This high degree of compatibility led to a reduced energy loss due to reflections, which ensures an efficient transmission and reception of electromagnetic waves. Furthermore, the antenna demonstrated a wide 10 dB bandwidth covering the frequency range from 2.1 GHz to 2.51 GHz. This wide bandwidth makes the suggested antenna a good choice for biomedical communication systems, where large data rates are essential. The combination of ultra-low reflection, near-perfect VSWR, and wide bandwidth confirms the antenna's suitability for advanced applications, such as imaging and wireless transmission in biomedical devices, where both performance and frequency coverage are critical.

4.2. Radiation Pattern

The gains of the three antenna configurations are presented in Fig. 8. The first antenna design in Fig. 8(a) showed a low gain of -5.42 dB, which indicates poor radiation and strong signal loss. In addition, the design 2 in Fig. 8(b), with one MTM unit cell, achieved an improved gain of 0.5 dB. This improvement confirms the big impact of design optimization. Finally, the final and proposed design in Fig. 8(c), which contained two unit cells, achieved a gain of 1.96 dB. This gain enhancement confirms the role of MTM in improving the radiation characteristics and overall antenna performance.

4.3. Directivity

The directivity of the suggested antenna stages is illustrated in Fig. 9. An enhancement in directivity was observed across the three designs, resulting in a final enhanced value of 3.18 dB for the proposed configuration. This obtained improvement highlights the impact of the integration of MTM structures to focus the radiated energy more directly in the desired direction.

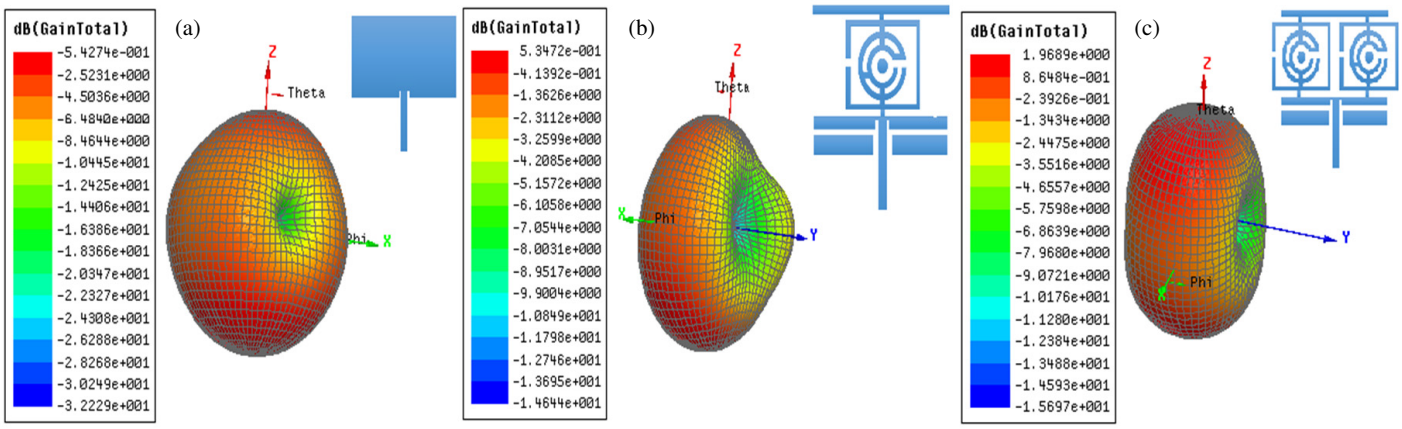

FIGURE 8. 3D gain; (a) simple patch, (b) with one cell, and (c) with two cells.

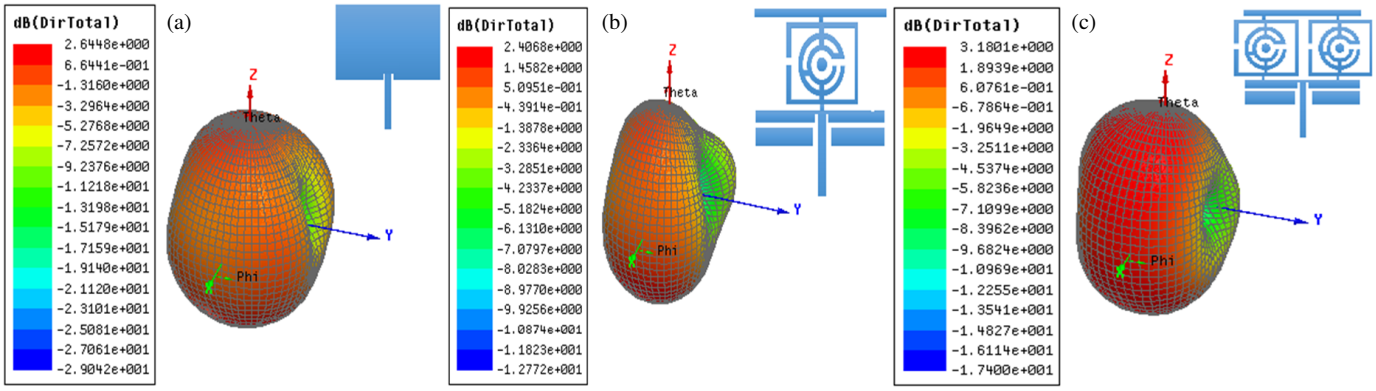

FIGURE 9. 3D directivity; (a) simple patch, (b) with one cell, and (c) with two cells.

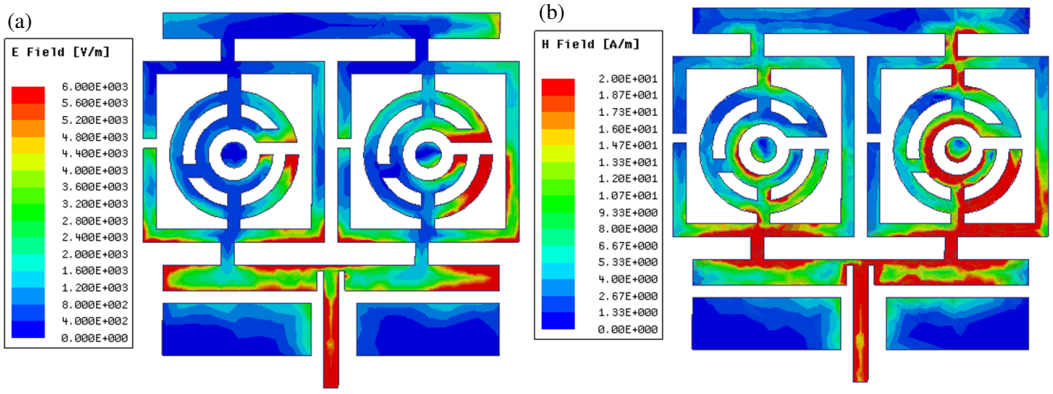

FIGURE 10. Proposed configuration; (a) electric field and (b) magnetic field.

4.4. Electric and Magnetic Distribution

The electric and magnetic field distributions of the proposed configuration at 2.48 GHz are illustrated in Fig. 10(a) and Fig. 10(b), respectively. The electric field achieved a strong and confined concentration around the two unit cells, with a peak value of 6×10^3 V/m, which indicates efficient excitation and coupling within the structure. Similarly, the magnetic field distribution is largely symmetric and uniform, with a maximum value of 2×10 A/m. This approximate symmetry and uniformity arise from the balanced geometry of the antenna and the uniform current distribution across the MTM unit cells, which ensures stable radiation behavior and effective magnetic response. These field characteristics confirm the performance enhancements achieved through the integration of MTM-based unit cells.

4.5. Antenna Fabricated Prototype

To validate and confirm the validity of the obtained results, a prototype of the proposed antenna was fabricated. The measurement setup was performed through the use of a calibrated

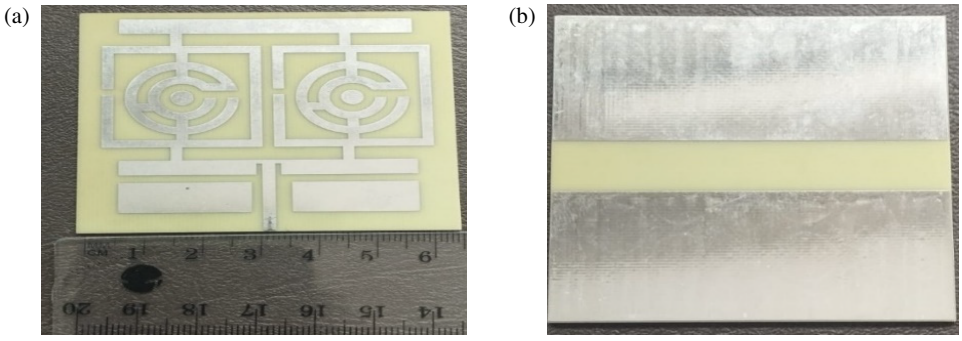

FIGURE 11. Antenna fabricated prototype; (a) top view, (b) bottom view.

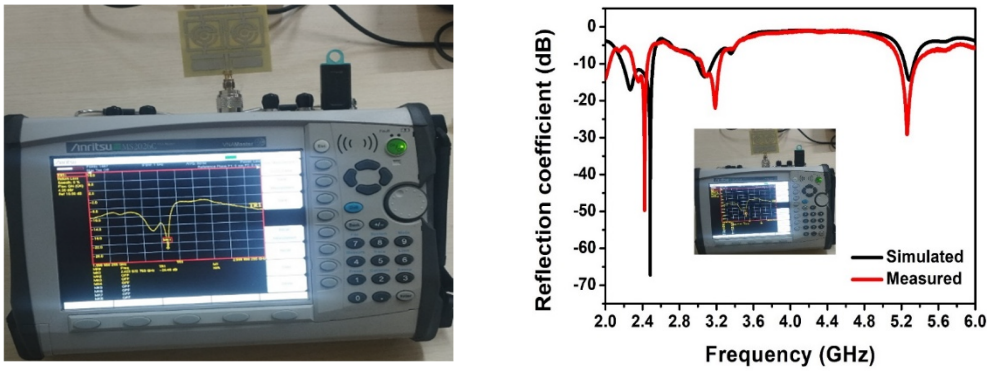

FIGURE 12. Antenna simulated and measured S_{11}.

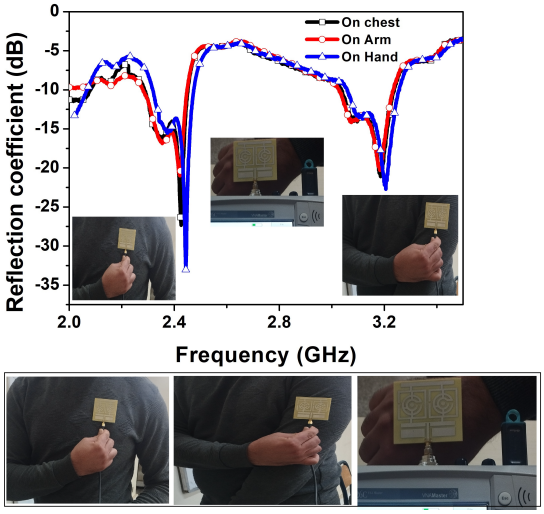

FIGURE 13. Measured antenna S_{11} on arm, on chest, and on hand.

vector network analyzer (VNA). To obtain better measurement precision, the VNA was calibrated employing a standard open-short-load-through (OSLT) technique.

The fabricated antenna prototype is presented in Fig. 11, while Fig. 12 presents a comparison of the simulated and measured S_{11} in free space. The measured results achieved an S_{11} value of -49.69 dB at the target frequency, with a very good agreement with the simulated results. This close correlation between the simulation and measurement confirms the accuracy of the simulation model and validates the robustness of the design and fabrication processes.

The performance of the fabricated antenna was also evaluated in practical cases by placing it on a human hand, chest, and arm. However, the measured S_{11} are illustrated in Fig. 13. The antenna achieved strong and consistent performance, with return loss values of -33.10 dB on the hand, -20.90 dB on the arm, and -27.35 dB on the chest, respectively. These results confirm the antenna's robustness and reliability, validating its suitability for wearable biomedical applications in real-world scenarios.

The Specific Absorption Rate (SAR) analysis was also taken into account to ensure compliance with international safety standards. The SAR was calculated using Computer Simulation Technology (CST) over a 10 g tissue volume with a human body model composed of three layers: skin, muscle, and fat as presented in Fig. 14(a). The value should be less than 2 W/kg following the IEEE/IEC guidelines. The results in Fig. 14(b) confirm that the SAR values remained well below the maximum permissible limits with a value of 1.49 W/kg (less than 2), validating the antenna's safe integration into wearable biomedical systems without posing health risks to the user.

The human body characteristics are listed in Table 3.

TABLE 3. Human body layers characteristics.

Tissue	Thickness (mm)	Dielectric ε_r	Conductivity σ (S/m)
Muscle	8	49	1.69
Fat	5	5	0.1
Skin	2	39	1.43

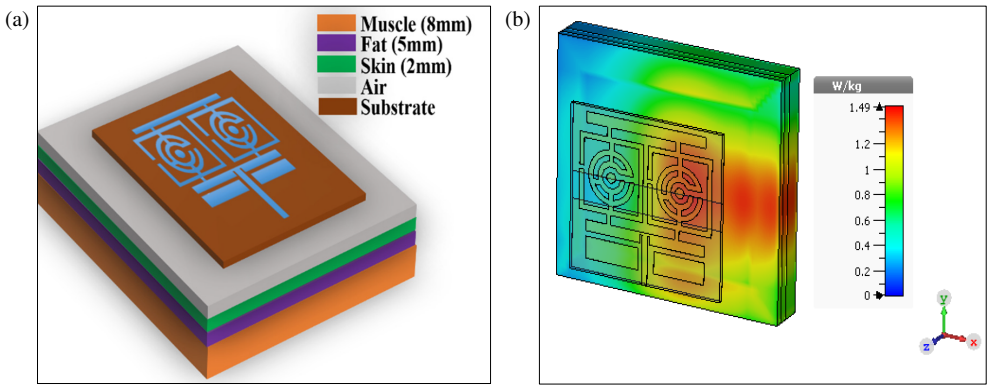

FIGURE 14. (a) Human body model, (b) antenna simulated SAR at 2.48 GHz.

TABLE 4. Comparison of the suggested antenna with previous published designs.

Ref.	Size	Substrate	Freq. (GHz)	Operating Band	S_{11} (dB)	VSWR	Application
[19]	$11 \times 10\,\text{cm}^2$	Polyester	2.45	2.38–2.52 GHz	−20.86	1.19	Biomedical
[20]	$75.85 \times 57.23\,\text{mm}^2$	FR4	2.42	2.39–2.45 GHz	−25.26	1.12	Wireless
[21]	$56.90 \times 56.90\,\text{mm}^2$	FR4	2.45	2.479–2.4197	−63.062	1.001	Biomedical
[22]	$28 \times 20\,\text{mm}^2$	FR4	2.4	ISM Band	−52.04	-	Biomedical
[23]	$100 \times 100\,\text{mm}^2$	FR4	2.45	2.41–2.48 GHz	−20.40	1.211	Wireless
[24]	$76 \times 59\,\text{mm}^2$	FR4	2.4	2.36–2.43 GHz	−44.78	1.013	-
This	$66 \times 60\,\text{mm}^2$	FR4	2.48	2.1–2.51 GHz	−67.20	1.01	Biomedical

Table 4 presents a comparison between the proposed antenna design and previously reported works. The comparison includes some important parameters, including antenna size, substrate type, resonance frequency, operating bandwidth, S_{11}, VSWR, and target application. The proposed design outperformed existing solutions by offering a more compact form factor, broader bandwidth, and improved impedance matching. These advantages highlight the effectiveness of the antenna and make it a strong candidate for modern wearable and biomedical applications.

5. CONCLUSION

This paper presents a compact 2.48 GHz patch antenna designed for biomedical applications. The antenna contained two unit cells on an FR4 substrate with a total size of $66 \times 60\,\text{mm}^2$. It demonstrated enhanced performance, with simulated and measured return losses of −67.20 dB and −49.69 dB, respectively, and excellent impedance matching, with a VSWR of 1.01. A prototype was fabricated in order to validate the simulation results, showing good agreement between the simulation and measurement results. To evaluate the validity of the antenna in real-world applications, the antenna was tested on a human hand, chest, and arm to simulate wearable use, such as integration into clothing. The results confirmed enhanced characteristics in proximity to the body, with an SAR value below 2 W/kg safety threshold, which supports its suitability for biomedical use. Future work will focus on link budget calculations.

REFERENCES

[1] Panda, S., A. Gupta, and B. Acharya, "Wearable microstrip patch antennas with different flexible substrates for health monitoring system," *Materials Today: Proceedings*, Vol. 45, 4002–4007, 2021.

[2] Gupta, V. and R. Kumar, "Biomedical telemetry antenna innovations: Progress, uses, and prospects for the future," *Progress In Electromagnetics Research B*, Vol. 106, 85–99, 2024.

[3] El Abbasi, M. K., M. Madi, H. F. Jelinek, and K. Y. Kabalan, "Wearable blood pressure sensing based on transmission coefficient scattering for microstrip patch antennas," *Sensors*, Vol. 22, No. 11, 3996, May 2022.

[4] Byun, G.-S., "A wireless data transfer by using a patch antenna for biomedical applications," *Electronics*, Vol. 11, No. 24, 4197, Dec. 2022.

[5] Zegadi, R., B. Lamine, S. Djamel, I. Elfergani, A. Varshney, M. Samira, B. R. Ibtissam, M. Said, J. Rodriguez, and C. Zebiri, "Study and analysis of a circular patch antenna for biomedical applications," in *Proceedings of the 3rd International Multi-Disciplinary Conference: Integrated Sciences and Technologies, IMDC-IST 2023*, 25–27, Yola, Nigeria, Oct. 2023.

[6] Venkatachalam, D., V. Jagadeesan, K. B. M. Ismail, M. A. Kumar, S. Mahalingam, and J. Kim, "Compact flexible planar antennas for biomedical applications: Insight into materials and systems design," *Bioengineering*, Vol. 10, No. 10, 1137, Sep. 2023.

[7] Uganya, G., R. M. Bommi, and A. M. J. Kinol, "Comparative analysis of microstrip patch antenna with different slots and substrate materials," in *2023 4th International Conference on Electronics and Sustainable Communication Systems (ICESC)*, 125–131, Coimbatore, India, Jul. 2023.

[8] Bouchachi, I., A. Reddaf, M. Boudjerda, K. Alhassoon, B. Babes, F. N. Alsunaydih, E. Ali, M. Alsharef, and F. Alsaleem, "Design and performances improvement of an UWB antenna with DGS structure using a grey wolf optimization algorithm," *Heliyon*, Vol. 10, No. 5, e26337, Mar. 2024.

[9] Younes, S. and F. Jaouad, "Wearable patch antenna with rectangular slots and defected ground for biomedical applications," in *2023 IEEE International Conference on Contemporary Computing and Communications (InC4)*, 1–6, Bangalore, India, Apr. 2023.

[10] Soerbakti, Y., R. F. Syahputra, M. D. H. Gamal, D. Irawan, E. H. Putra, R. S. Darwis, *et al.*, "Improvement of low-profile microstrip antenna performance by hexagonal-shaped SRR structure with DNG metamaterial characteristic as UWB application," *Alexandria Engineering Journal*, Vol. 61, No. 6, 4241–4252, Jun. 2022.

[11] Lima, A. M., N. H. O. Cunha, and J. P. da Silva, "Effect of metamaterial cells array on a microstrip patch antenna design," *Journal of Microwaves, Optoelectronics and Electromagnetic Applications*, Vol. 19, No. 3, 327–342, Sep. 2020.

[12] Siraj, Y., Y. Khardioui, K. S. Alaoui, and J. Foshi, "High-performance terahertz patch antenna with metamaterials for advanced 6G and biomedical technologies," *Scientific African*, Vol. 28, e02716, Jun. 2025.

[13] Chen, C., Y. He, Y. Chen, G. Lu, M.-H. Lu, and X. Li, "Impact dynamics of mechanical metamaterials: A short review and perspective," *Forces in Mechanics*, Vol. 21, 100335, Dec. 2025.

[14] Das, G. K., S. Basu, B. Mandal, D. Mitra, R. Augustine, and M. Mitra, "Gain-enhancement technique for wearable patch antenna using grounded metamaterial," *IET Microwaves, Antennas & Propagation*, Vol. 14, No. 15, 2045–2052, Dec. 2020.

[15] Ajewole, B., P. Kumar, and T. Afullo, "A microstrip antenna using I-shaped metamaterial superstrate with enhanced gain for multiband wireless systems," *Micromachines*, Vol. 14, No. 2, 412, Feb. 2023.

[16] Satarkar, P. R. and R. B. Lohani, "Characterization of metamaterial based patch antenna for worldwide interoperability for microwave access application," *Bulletin of Electrical Engineering and Informatics*, Vol. 11, No. 5, 2687–2695, 2022.

[17] Gudibandi, B. R. and M. Muniyandi, "A high magnetic permeability metamaterial superstrate as a gradient index lens for 2.4 GHz patch antenna gain enhancement," *Journal of Magnetism and Magnetic Materials*, Vol. 626, 173089, Aug. 2025.

[18] Rothwell, E. J., J. L. Frasch, S. M. Ellison, P. Chahal, and R. O. Ouedraogo, "Analysis of the Nicolson-Ross-Weir method for characterizing the electromagnetic properties of engineered materials," *Progress In Electromagnetics Research*, Vol. 157, 31–47, 2016.

[19] Didi, S.-E., I. Halkhams, A. Es-Saqy, M. Fattah, S. Mazer, and M. El Bekkali, "Creation of a soft circular patch antenna for biomedical applications for 5G at frequency 2.45 GHz," *Results in Engineering*, Vol. 22, 102319, Jun. 2024.

[20] Abdulhussein, A. M., A. H. Khidhi, and A. A. Naser, "Omnidirectional microstrip patch antenna for 2.4 GHz wireless communications," *Journal of Physics: Conference Series*, Vol. 2114, No. 1, 012051, 2021.

[21] Akbar, M. A., S. Chakraborty, A. J. Islam, M. M. Farhad, and M. M. Gani, "Performance analysis of a microstrip patch antenna for biomedical applications," in *2019 International Conference on Electrical, Computer and Communication Engineering (ECCE)*, 1–6, Cox'sBazar, Bangladesh, Feb. 2019.

[22] Ramli, N. H., H. Othman, and D. K. Hamzah, "Design a CPW fed implantable antenna at frequency 2.4 GHz for wireless implantable body area network," *IOP Conference Series: Materials Science and Engineering*, Vol. 932, No. 1, 012071, 2020.

[23] Rana, M. S., B. K. Sen, M. T.-A. Mamun, M. S. Mahmud, and M. M. Rahman, "A 2.45 GHz microstrip patch antenna design, simulation, and analysis for wireless applications," *Bulletin of Electrical Engineering and Informatics*, Vol. 12, No. 4, 2173–2184, 2023.

[24] Şeker, C. and M. T. Güneşer, "Design and simulation of 26 GHz patch antenna for 5G mobile handset," in *2019 11th International Conference on Electrical and Electronics Engineering (ELECO)*, 676–678, Bursa, Turkey, Nov. 2019.